

# Revealing the Origin of Neutrino Masses through Displaced Shower Searches in the CMS Muon System

Wei Liu,<sup>1,\*</sup> Suchita Kulkarni,<sup>2,†</sup> and Frank F. Deppisch<sup>3,‡</sup>

<sup>1</sup>*Department of Applied Physics and MIIT Key Laboratory of Semiconductor Microstructure and Quantum Sensing, Nanjing University of Science and Technology, Nanjing 210094, China*

<sup>2</sup>*Institute of Physics, NAWI Graz, University of Graz, Universitätsplatz 5, A-8010 Graz, Austria*

<sup>3</sup>*University College London, Gower Street, London WC1E 6BT, United Kingdom*

We study the potential to probe the origin of neutrino masses, by searching for long-lived right-handed neutrinos (RHNs)  $N$  in the  $B-L$  gauge model. Despite the small active-sterile mixing  $|V_{\ell N}|^2$ , RHNs are produced abundantly via SM and exotic Higgs production, as long as the Higgs mixing is sufficiently large. We reinterpret a search for displaced showers in the CMS muon system and we find that it is sensitive to parameter space at and below the canonical seesaw floor,  $|V_{\ell N}|^2 \approx 10^{-12}$  ( $\ell = e, \tau$ ) for  $m_N \approx 40$  GeV. With existing data constraining such a well-motivated scenario of neutrino mass generation, we determine the projected sensitivity at the HL-LHC, motivating dedicated searches for long-lived RHNs with decay lengths  $\approx 10$  m.

## I. INTRODUCTION

The Standard Model of particle physics cannot explain the observed neutrino masses, which have been confirmed in neutrino oscillations [1–3]. The most popular scenario to explain the presence of small neutrino masses is through the seesaw mechanism [4] where heavy right-handed neutrinos (RHNs) are introduced. Through their Yukawa couplings with the Standard Model (SM) Higgs and the active neutrinos, light neutrino masses are induced. This mechanism can also generate the observed matter-antimatter asymmetry of the Universe through leptogenesis [5–7].

If the RHN masses  $m_N$  are of the order of the electroweak (EW) scale, the active-sterile mixing

---

\*Electronic address: [wei.liu@njust.edu.cn](mailto:wei.liu@njust.edu.cn)

†Electronic address: [suchita.kulkarni@uni-graz.at](mailto:suchita.kulkarni@uni-graz.at)

‡Electronic address: [f.deppisch@ucl.ac.uk](mailto:f.deppisch@ucl.ac.uk)

strength  $V_{\ell N}$  required to generate the SM neutrino mass  $m_\nu \lesssim 0.4$  eV is  $|V_{\ell N}|^2 \sim m_\nu/m_N \lesssim 10^{-11} \times (40 \text{ GeV}/m_N)$ . Long-lived RHNs are produced at colliders via this weak active-sterile neutrino mixing. Given the displaced signature coupled with low backgrounds, RHNs have received increased attention in phenomenological studies [8–15]. Numerous experimental searches for RHNs have been carried out [16–28], with recent summaries in [12, 29]. The resulting limits on the active-sterile mixing are  $|V_{\ell N}|^2 \lesssim 10^{-5}$  for  $m_N \approx 10$  GeV.

While suggestive, the seesaw mechanism does not explain the origin of the RHN Majorana masses. Arguably the most direct scenario to remedy this is the  $B - L$  (baryon - lepton number) gauge model [30, 31]; it generates RHN Majorana masses through the spontaneous breaking of a  $U(1)_{B-L}$  gauge symmetry. The origin of heavy neutrino masses is thus analogous to that in SM EW symmetry breaking. The inclusion of three RHNs  $N_i$ , in addition to the exotic gauge boson  $Z'$  and  $B - L$ -breaking Higgs  $\Phi$  makes this model free of quantum anomalies. The RHNs may also generate the baryon asymmetry of the universe via leptogenesis [15] and the  $B - L$  model can be made conformally invariant. This could not only explain why the symmetry is broken near the TeV scale but could also induce EW symmetry breaking [32, 33]. In such a scenario, primordial black holes may explain Dark Matter [34]. RHNs in the  $B - L$  model not only interact with the SM particles via the active-sterile neutrino mixing  $V_{\ell N}$ , but also through the  $B - L$  gauge and Higgs portals.

Thus, RHNs can also be produced via the SM Higgs, the  $B - L$  Higgs as well as the SM  $Z$  and  $B - L$   $Z'$ . In these channels, the production is independent of the active-sterile mixing strength. Hence, the RHN can be abundantly produced if either the Higgs mixing or the  $B - L$  gauge coupling are large. It is well known that enabling these portals allows testing active-sterile mixing strengths [35–58]. This is because the RHN decay still proceeds via  $|V_{\ell N}|$  ( $\ell = e, \mu, \tau$ ), i.e.,  $N \rightarrow \nu_\ell h, \nu_\ell Z^*, \ell W^*$ , where the off-shell SM  $h, Z$  and  $W$  decay via SM particles. The total decay width is thus suppressed by the active-sterile mixing, leading to macroscopic proper decay lengths ( $m_N < m_{W,Z}$ ) [59],

$$L_N^0 \approx 3 \text{ m} \times \left( \frac{10^{-12}}{|V_{\ell N}|^2} \right) \left( \frac{40 \text{ GeV}}{m_N} \right)^5. \quad (1)$$

Long-lived particles (LLPs), such as the RHNs in our scenario, can be searched for at existing Large Hadron Collider (LHC) detectors. We here focus on a search for displaced showers in the CMS muon system [60], specifically the muon endcap detectors furthest from the interaction point.

Such displaced showers originate when the LLP decays to photons, electrons, taus or quarks. The original search was for a generic scalar LLP  $S$ , pair-produced via the SM Higgs,  $pp \rightarrow h \rightarrow SS$  and decaying to bottom quarks, down quarks or  $\tau$  leptons. It provides the most stringent limits for long LLP proper decay lengths of  $6 - 40$  m and LLP masses of  $7 - 40$  GeV. Similarly, ATLAS searched for hadronic LLP decays [61–63], with weaker limits. ATLAS search [63] has also been reinterpreted for pair production of HNL [64]. The CMS muon endcap search has been considered in [65] for sterile neutrinos. We instead reinterpret it in the  $B - L$  gauge model. We especially focus on Higgs production and we find that it is sensitive to the canonical seesaw floor, i.e., for active-sterile mixing strengths required to generate the light neutrino masses. While the  $B - L$  gauge model clearly makes more assumptions, and large enough Higgs mixing is required, our analysis shows for the first time that existing data from the LHC probes the origin of neutrino masses in a well motivated scenario.

This paper is organized as follows. In Sec. II, we compare the different RHN production and decay channels. Our reinterpretation of the CMS muon endcap search is discussed in Sec. III. We present our results in Sec. IV, demonstrating that existing data is probing the canonical seesaw floor. We conclude in Sec. V.

## II. RIGHT-HANDED NEUTRINO PRODUCTION AND DECAY

The  $B - L$  gauge model extends the SM gauge group by an Abelian gauge symmetry  $U(1)_{B-L}$ . The SM fermions carry their canonical  $Q_{B-L}$  charges and the three RHNs  $N_i$  have a  $Q_{B-L} = -1$  but are otherwise sterile. The  $B - L$  symmetry is spontaneously broken by the vacuum expectation value (VEV) of a SM singlet Higgs  $\Phi$  with  $Q_{B-L} = 2$ . This results in a heavy  $Z'$  gauge boson and heavy Majorana RHNs. The relevant features of the  $B - L$  gauge model are summarized in Appendix A, where we also review constraints. To emphasize the principle of our approach we assume that a single RHN  $N$  is light enough to be produced and that it mixes dominantly with a single lepton flavour  $\ell$  at a time through the active-sterile mixing  $V_{\ell N}$ . As the SM background for muons is overwhelming in the muon chamber, we concentrate on  $\ell = e, \tau$  [65].

We first compare the four resonant RHN production channels at the LHC, namely via the  $Z'$ , SM  $Z$ , SM-like Higgs  $h$  and  $(B - L)$ -like Higgs  $\Phi$ . We omit production via the SM charged and neutral currents as they are suppressed by the small active-sterile mixing  $|V_{\ell N}|$ . The RHNs instead

decay to SM particles via these currents while contributions from  $Z'$ ,  $h$  and  $\Phi$  are negligible. The dominant channels are  $N \rightarrow \ell W \rightarrow \ell q \bar{q}, \ell \ell \nu$ ,  $N \rightarrow \ell^\pm \ell^\mp \nu$ . As we consider light RHNs,  $m_N < m_{W,Z}$ , they undergo 3-body decays with the proper decay length given in Eq. (1). At the canonical seesaw floor, the RHNs thus have proper decay lengths  $L_N^0 \approx \mathcal{O}(10)$  m.

The produced RHNs are boosted, increasing the observed decay length to  $L_N = \beta \gamma L_N^0$ , with an average boost factor of  $\langle \beta \gamma \rangle \approx 1 - 10$ . Such long decay lengths are best probed in detectors far away from the interaction point (IP). This motivates the use of the muon system as it forms the outer layer of the CMS detector at a distance of  $\approx 8 - 13$  m from the IP.

### A. Gauge Portal

With quarks and RHNs charged under  $B - L$ , the most direct channel to produce RHNs at the LHC is through the  $Z'$  gauge portal,  $pp \rightarrow Z' \rightarrow NN$ . As a benchmark, we will later use  $m_{Z'} = 500$  GeV and the production cross section at the 13 TeV LHC is  $\sigma(pp \rightarrow Z' \rightarrow NN) = \sigma(pp \rightarrow Z') \times \text{Br}(Z' \rightarrow NN)$ , with  $\sigma(pp \rightarrow Z') \approx 0.4 \text{ fb} \times (g_{B-L}/10^{-3})^2$ . The branching ratio is  $\text{Br}(Z' \rightarrow NN) \approx 1/13$  for  $m_N \ll m_{Z'}$ , leading to a total cross section of

$$\sigma(pp \rightarrow Z'(500) \rightarrow NN) \approx 0.75 \text{ fb} \times \left( \frac{g_{B-L}}{5 \times 10^{-3}} \right)^2. \quad (2)$$

The most stringent limit from ATLAS resonance searches [66] is  $g_{B-L} \lesssim 0.005$  for  $m_{Z'} = 500$  GeV.

The SM  $Z$  can mix with the  $Z'$ , inducing the SM gauge portal  $pp \rightarrow Z \rightarrow NN$ , controlled by the effective coupling  $\beta = g_{B-L} \sin \theta_{ZZ'}$ . The SM cross section at the 13 TeV LHC is  $\sigma(pp \rightarrow Z) \approx 5.8 \times 10^7 \text{ fb}$  [67], and the decay branching ratio is  $\text{Br}(Z \rightarrow NN) \approx 0.48 \times \beta^2$  for  $m_N \ll m_Z$ . This results in a total cross section of

$$\sigma(pp \rightarrow Z \rightarrow NN) \approx 28 \text{ fb} \times \left( \frac{\beta}{10^{-3}} \right)^2. \quad (3)$$

Limits from atomic parity violation are of the order  $\beta \lesssim 10^{-3}$  [68].

### B. Higgs Portal

The SM Higgs and the  $B - L$  Higgs also mix, described by the Higgs mixing parameter  $\sin \alpha$ . RHNs can then be produced via the SM Higgs,  $pp \rightarrow h \rightarrow NN$ , where we only consider gluon-gluon

fusion; while vector boson fusion and associated Higgs production are also possible, they contribute at most 10% to the overall cross section [69] and the resulting final states are unlikely to pass our trigger requirements. The  $pp \rightarrow h \rightarrow NN$  production cross section is then  $\sigma(pp \rightarrow h \rightarrow NN) = \cos^2 \alpha \times \sigma(pp \rightarrow h)_{\text{SM}} \times \text{Br}(h \rightarrow NN)$  [49, 51]. Here,  $\sigma(pp \rightarrow h)_{\text{SM}} = 44 \pm 4$  pb ( $50 \pm 7$  pb) is the SM Higgs production cross section at the 13 TeV (14 TeV) LHC via gluon-gluon fusion [69, 70]. The branching ratio can be approximated as [51]

$$\text{Br}(h \rightarrow NN) \approx \frac{\tan^2 \alpha}{16\pi} \frac{m_N^2}{\langle \Phi \rangle^2} \frac{m_h}{\Gamma_h^{\text{SM}}} \left(1 - \frac{4m_N^2}{m_h^2}\right)^{3/2}, \quad (4)$$

with the SM Higgs decay width  $\Gamma_h^{\text{SM}} \approx 4.1$  MeV [71]. It is suppressed by  $\sin \alpha$  and the RHN Yukawa coupling with the  $B-L$  Higgs  $\Phi$ ,  $y_N = m_N/\langle \Phi \rangle = 2g_{B-L}m_N/m_{Z'}$ . The cross section is maximized for  $m_N = m_h/\sqrt{10} \approx 40$  GeV,

$$\sigma(pp \rightarrow h \rightarrow NN) \lesssim 7.8 \text{ fb} \times \left(\frac{\sin \alpha}{0.1}\right)^2 \left(\frac{5 \text{ TeV}}{\langle \Phi \rangle}\right)^2. \quad (5)$$

Both the Higgs mixing  $\sin \alpha$  and the  $(B-L)$  VEV  $\langle \Phi \rangle$  are experimentally constrained through direct and indirect Higgs probes and  $Z'$  searches, respectively. In our analysis, we choose  $\langle \Phi \rangle = 3.75$  TeV. This is above the current lower limit from EW precision tests,  $\langle \Phi \rangle \gtrsim 3.5$  TeV [72, 73].

Similarly, RHNs can be produced via the  $B-L$  Higgs  $\Phi$ . This time, the SM quarks and gluons will couple to  $\Phi$  with a suppression as  $\sigma(pp \rightarrow \Phi \rightarrow NN) \approx \sin^2 \alpha \times \sigma(pp \rightarrow \Phi)_{\text{SM}} \times \text{Br}(\Phi \rightarrow NN)$ , where  $\sigma(pp \rightarrow \Phi)_{\text{SM}}$  is the production cross section treating  $\Phi$  as the SM Higgs but with mass  $m_\Phi$ . The  $B-L$  Higgs decays to heavy SM fermions and boson pairs via mixing to the SM Higgs, and RHN pairs via the Yukawa coupling  $y_N$ . For  $m_\Phi < 2m_W$ , the branching ratio to RHN pairs is

$$\text{Br}(\Phi \rightarrow NN) = \frac{\Gamma(\Phi \rightarrow NN)}{\sin^2 \alpha \Gamma_\Phi^{\text{SM}} + \Gamma(\Phi \rightarrow NN)}, \quad (6)$$

where  $\Gamma_\Phi^{\text{SM}}$  is the total decay width treating  $\Phi$  as the SM Higgs but with mass  $m_\Phi$ , and the partial width is  $\Gamma(\Phi \rightarrow NN) = \cos^2 \alpha / (16\pi) m_N^2 m_\Phi / \langle \Phi \rangle^2$  for  $m_N \ll m_\Phi$  [55]. This results in the 13 TeV LHC cross section

$$\sigma(pp \rightarrow \Phi(150) \rightarrow NN) \lesssim 100 \text{ fb} \times \left(\frac{5 \text{ TeV}}{\langle \Phi \rangle}\right)^2, \quad (7)$$

for  $m_\Phi < 2m_W \approx 160$  GeV. For  $m_\Phi \gtrsim 2m_{W,Z} \approx 200$  GeV, the decays  $\Phi \rightarrow WW, ZZ$  dominate, giving

$$\sigma(pp \rightarrow \Phi(200) \rightarrow NN) \lesssim 1 \text{ fb} \times \left(\frac{5 \text{ TeV}}{\langle \Phi \rangle}\right)^2. \quad (8)$$

The cross section decreases rapidly with larger  $m_\Phi$  and we use  $m_\Phi = 150$  GeV as benchmark in the following.

### III. DISPLACED SHOWERS IN THE CMS MUON SYSTEM

The above gives the overall rate expected but we require a detailed simulation to match the CMS endcap search. To this end, the model is implemented as a Universal FeynRules Output (UFO) [74], following [37, 49]. The Monte Carlo event generator MadGraph5aMC@NLO v3.4.1 [75] is then used for a parton level simulation of the events with the shower jets and matrix element jets matched [76, 77] with  $X_{qcut} = 40$  GeV. Events are fed to PYTHIA v8.235 [78] for initial and final state parton showering, hadronization and heavy hadron decays. Clustering of events is performed by FastJet v3.2.1 [72] and the hadron level events are simulated at the detector level with Delphes v3.5.1 [79].

We determine the sensitivity of the CMS search [60], which uses the muon detector as a sampling calorimeter to identify showers produced by the decays of an LLP. An update to this search is available [80]. However, detailed reinterpretation information is, as of yet, missing. We do not expect this to have a large impact as the triggers are largely the same. The decays produce photons, electrons, tau or quarks inside the muon detector creating hadronic and electromagnetic showers and giving rise to a large number of hits in a small region of the detector as the showers are collimated. These hits are identified by cathode strip chambers (CSCs), which detect charged particles via ionisation of gas molecules and they are clustered by identifying high-density regions. Such clusters are called CSC clusters. Using this strategy, the CMS search detects electromagnetic and hadronic energy from electrons, taus, photons and jets but it does not include muons as they rarely produce particle showers. As the search strategy relies on identification and reconstruction of original information using CSC clusters, to aid reinterpretation of the search, CMS provides an updated card and modules for the Delphes detector simulation [60, 81, 82]. We implement these to determine the reconstruction efficiency and kinematic information of the CSC cluster events, and apply the selection criteria of the CMS search:

The *missing transverse energy* is  $E_T^{\text{miss}} > 200$  GeV as trigger requirement. The missing transverse energy is defined as the negative vector sum of visible  $p_T$  energy deposited in the tracker and calorimeter. If the signal contains only LLPs which decay beyond the calorimeter, there is no missing energy to trigger on. We thus simulate the signal up to two initial state jets, which are

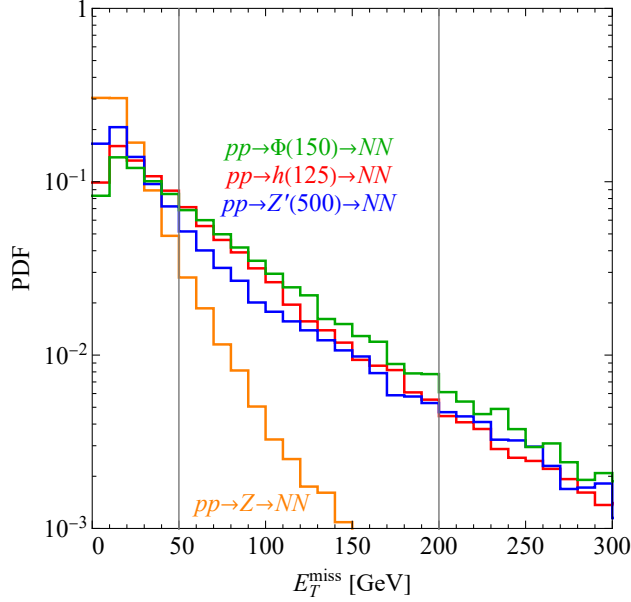


FIG. 1: Missing transverse energy  $E_T^{\text{miss}}$  for  $pp \rightarrow Z' \rightarrow NN$  ( $m_{Z'} = 500$  GeV, blue),  $pp \rightarrow Z \rightarrow NN$  (green),  $pp \rightarrow h \rightarrow NN$  (red) and  $pp \rightarrow \Phi \rightarrow NN$  ( $m_\Phi = 150$  GeV, orange), with  $m_N = 30$  GeV and  $|V_{\ell N}|^2 = 10^{-12}$ . The vertical dashed lines indicate the thresholds  $E_T^{\text{miss}} > 200$  GeV and  $> 50$  GeV in the CMS search and the soft trigger strategy, respectively.

prompt and deposit energy in the calorimeter.

*No electron (muon) with transverse momentum  $p_T > 35$  (25) GeV and pseudorapidity  $|\eta| < 2.5$  (2.4), to remove background from  $W$  and top production.*

*At least one CSC cluster with  $|\Delta\phi(\mathbf{x}_{\text{CSC}}, \mathbf{p}_T^{\text{miss}})| < 0.75$  to ensure that the cluster originated from the LLP decay. Here,  $\Delta\phi$  is defined as the azimuthal angle between the missing transverse momentum and the cluster location from the IP. This ensures that the LLP is close to the direction of missing energy, which points in the opposite direction of the vector sum of the visible  $p_T$ .*

*Events with clusters too close to a jet (muon) are removed, for  $\Delta R = \sqrt{(\Delta\eta)^2 + (\Delta\phi)^2} < 0.4$ . This ensures that the CSC cluster is not matched to jets (muons) with  $p_T > 10$  (20) GeV and the it is not created by LLPs inside the jet, e.g.  $K_L$ , or muon bremsstrahlung.*

*The average time of detector hits in the CSC cluster, relative to the time of collision is  $-5$  ns  $< \langle \Delta t_{\text{CSC}} \rangle < 12.5$  ns, to reject clusters produced by pileup.*

Due to  $E_T^{\text{miss}} > 200$  GeV, only a small number of signal events passes the selection criteria. This is illustrated in Fig. 1, showing the corresponding distribution for our production modes. The rate

drops rapidly for larger  $E_T^{\text{miss}}$ , especially for SM  $Z$  production, due to the fact that the missing transverse energy either originates from initial state radiation, which is enhanced for Higgs gluon-gluon fusion, or from heavier resonant particle masses, as in the  $Z'$  and  $\Phi$  modes. Nevertheless, only  $\approx 1\%$  of events satisfy the trigger requirement. In the SM  $Z$  mode, only  $\lesssim 0.1\%$  pass the trigger and we thus expect no appreciable sensitivity in this case.

To calculate the dominant gluon-gluon fusion Higgs production, we use the effective gluon-gluon-Higgs coupling at leading order [83]. We have checked that this is accurate for our purposes, giving a conservative determination; while the transverse momentum of the Higgs can significantly change when including higher order corrections [84, 85], by comparing the leading order effective treatment with the next-to-leading order fully resolved top quark mass-dependent vertex model [86], the effective model leads to a softer Higgs for  $p_T < 200$  GeV, while the distributions are comparable for  $200 < p_T < 400$  GeV. For  $p_T > 400$  GeV, the effective model overestimates by more than a factor of two. Nevertheless, as its cross section is roughly an order of magnitude smaller than for  $200 < p_T < 400$  GeV, we consider our calculation accurate for  $p_T > 200$  GeV.

In Ref. [65], it is argued that the CMS search could be improved as a search for sterile RHNs by assuming a dedicated Level-1 and a high-level displaced signature trigger. The requirement on  $E_T^{\text{miss}}$  can then be relaxed to  $E_T^{\text{miss}} > 50$  GeV, resulting in an improved signal rate by about an order of magnitude, cf. Fig. 1, while the background can still be controlled by requiring larger CSC clusters. We will refer to this option as the ‘soft trigger strategy’ in the following. The softened  $E_T^{\text{miss}}$  threshold means that we are more susceptible to Higgs production corrections as we are probing softer Higgs  $p_T$ . Our results are conservative as we underestimate the Higgs  $p_T$  distribution by about a factor of two.

We simulate the displaced shower signature at the 13 TeV LHC with  $137 \text{ fb}^{-1}$  of integrated luminosity and the 14 TeV HL-LHC with  $3000 \text{ fb}^{-1}$ . The background mainly comes from punch-through jets and muon bremsstrahlung, controlled by the above selection criteria and determined from CMS data in [60]: The number of expected background events is  $b = 2.0 \pm 1.0$  and the number of observed events is  $N = 3$ . excluding an expected number of signal events of  $s > 6.13$  at 95% confidence level (CL). At the HL-LHC, after taking into account a 20% (60%) signal loss due to pileup, and requiring more hits to control the background,  $s > 56$  (3) is required at 95 % CL with the CMS (soft) trigger strategy [65]. For the HL-LHC projection, we assume  $b = 40$  background



events at the HL-LHC for the CMS trigger and no background for the soft trigger.

#### IV. PROBING THE NEUTRINO MASS GENERATION MECHANISM

Using the above simulation strategy, we reinterpret the CMS search [60] in the  $B - L$  model, specifically to constrain or probe the RHN mass  $m_N$  and the active-sterile mixing  $|V_{\ell N}|$  for successful neutrino mass generation. In our simplified model with a single RHN  $N$ , a light neutrino acquires a Majorana mass  $m_\nu = |V_{\ell N}|^2 m_N$ . The KATRIN experiment limits the effective  $\beta$  decay neutrino mass as  $m_\beta < 0.45$  eV at 90 % CL [87], whereas solar neutrino oscillations point towards a neutrino mass scale of  $\sqrt{\Delta m_{\text{sol}}^2} = 9 \times 10^{-3}$  eV [88]. We take the range  $9 \times 10^{-3}$  eV  $< |V_{\ell N}|^2 m_N < 0.45$  eV as a target to probe the canonical seesaw floor of neutrino mass generation. We only consider active-sterile mixing to  $\ell = e, \tau$  flavour since the CMS muon detector cannot respond to displaced muons.

##### A. Gauge Portal

We start with the  $Z'$  gauge portal  $pp \rightarrow Z' \rightarrow NN$  where we use the benchmark values  $m_{Z'} = 500$  GeV and  $g_{B-L} = 0.005$ , satisfying current constraints. No sensitivity to the neutrino mass generation parameters is obtained in this case using the current CMS data with either the original or the soft trigger strategy, since the strong requirement on  $E_T^{\text{miss}}$  cuts away most of the signal. At the HL-LHC with  $3000 \text{ fb}^{-1}$ , our reinterpretation also only predicts a sensitivity for the soft trigger strategy. If the  $B - L$  gauge coupling is larger than  $g_{B-L} \gtrsim 0.0035$ , RHNs can be probed in this case, within the mass range  $10 \text{ GeV} \lesssim m_N \lesssim 80 \text{ GeV}$ .

Prospects for the SM gauge portal  $pp \rightarrow Z \rightarrow NN$  are similar. For a  $ZZ'$  mixing  $\beta = 10^{-3}$  at the current upper limit, no sensitivity at 95 % CL is achieved using current data. It can only be probed at the HL-LHC using the soft trigger strategy, for  $m_N \lesssim 40$  GeV. While the total cross section for the SM  $Z$  is sizeable as discussed in Sec. II, Fig. 1 demonstrates that a large number of events from  $Z$  production are removed due to small  $E_T^{\text{miss}}$ .

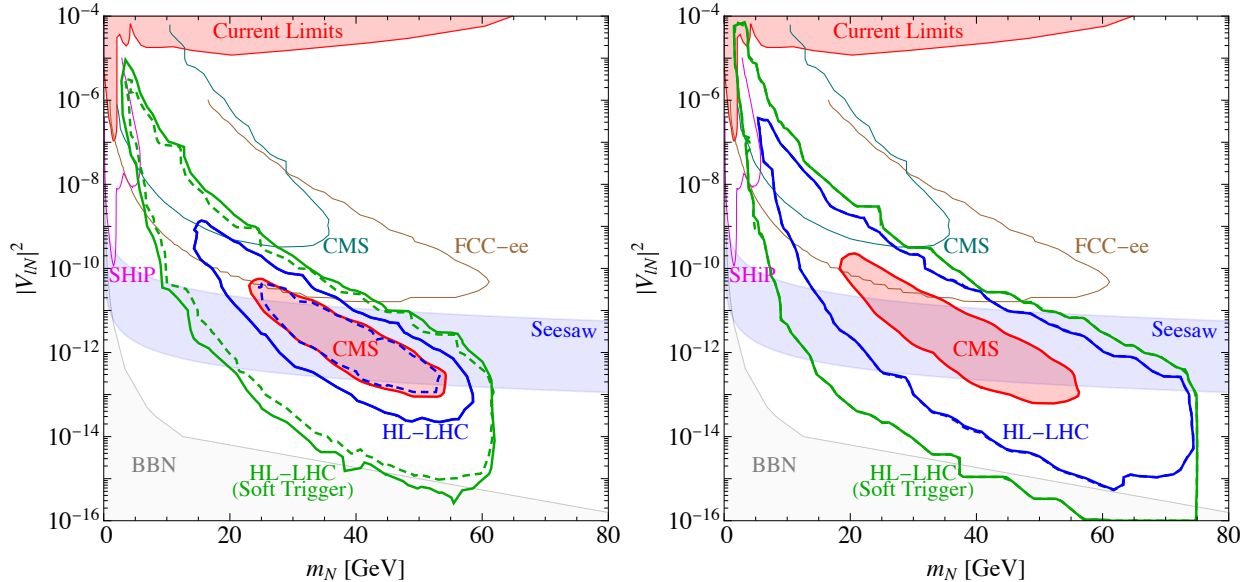


FIG. 2: Sensitivity of  $pp \rightarrow h \rightarrow NN$  (left) and  $pp \rightarrow \Phi \rightarrow NN$  (right,  $m_\Phi = 150$  GeV) at 95% CL on the RHN mass  $m_N$  and the active-sterile mixing  $|V_{\ell N}|^2$  ( $\ell = e, \tau$ ) using displaced shower searches in the CMS muon system. The scenarios are for the reinterpretation of the CMS data (red region), as well as the 14 TeV HL-LHC with  $3000 \text{ fb}^{-1}$  using the CMS (blue contours) and soft (red contours) trigger strategies. The Higgs mixing is fixed at  $\sin \alpha = 0.24$  (red region and solid contours) and 0.14 (dashed). The  $B - L$  Higgs VEV is fixed at  $\langle \Phi \rangle = 3.75$  TeV. The region labelled 'Current Limits' is excluded by existing sterile neutrino searches ( $\ell = e$ ) while the contours labelled SHiP, CMS and FCC-ee give the projected sensitivity of planned experiments to sterile neutrinos, compiled in [29, 89]. The band labelled 'Seesaw' indicates where  $9 \times 10^{-3} \text{ eV} < |V_{\ell N}|^2 m_N < 0.45 \text{ eV}$ .

## B. Higgs Portal

The prospects for the Higgs portals are much more promising. Applying the above analysis to the SM Higgs case,  $pp \rightarrow h \rightarrow NN$ , reinterpreting the CMS search, we find that existing CMS data already constrains the parameter space for light neutrino mass generation in the  $B - L$  gauge model. This is shown in Fig. 2 (left), where the red region labelled 'CMS' is excluded at 95% CL, for a Higgs mixing  $\sin \alpha = 0.24$  and  $B - L$  VEV  $\langle \Phi \rangle = 3.75$  TeV. As anticipated in Sec. II B, the sensitivity is maximal for  $m_N \approx m_h/\sqrt{10} \approx 40$  GeV. For a displaced search at distances  $\mathcal{O}(1 \text{ m})$  in the CMS muon system, this corresponds to the well-motivated canonical seesaw prediction  $|V_{\ell N}|^2 \approx 10^{-12}$  that is being probed.

Fig. 2 (left) also shows the projected sensitivity at the HL-LHC using the CMS (solid blue contour) and soft trigger (solid red contour) strategies. This extends the coverage of the seesaw regime over a broader range, up to  $10 \text{ GeV} \lesssim m_N \lesssim 60 \text{ GeV}$ . The HL-LHC will improve the sensitivity to the Higgs mixing, to values  $\sin \alpha \gtrsim 0.14$  [90, 91]. Using this value, i.e., assuming the HL-LHC will see no sign of the Higgs mixing with an exotic state, the sensitivity decreases to the dashed contours in Fig. 2 (left). In the three scenarios thus considered, the smallest  $\sin \alpha$  for which part of the seesaw region can be probed at 95% CL is  $\sin \alpha > 0.17$  (CMS reinterpretation), 0.1 (HL-LHC with CMS trigger) and 0.017 (HL-LHC with soft trigger).

In a broader context, beyond the scope of the  $B - L$  model, this result can also be interpreted in terms of the operator  $\mathcal{O}_{NH} = (\overline{N^c}N)(H^\dagger H)/\Lambda_{\text{NP}}$  in the RHN-extended SM effective field theory [92], assuming that there are no other exotic light degrees of freedom other than the RHN. After EW symmetry breaking it leads to the vertex  $(v/\Lambda_{\text{NP}})hNN$ , which will allow the SM Higgs to decay to RHNs. Matching the vertex factor with that in the  $B - L$  model,  $v/\Lambda_{\text{NP}} = y_N \sin \alpha/2 = m_N \sin \alpha/(2\langle\Phi\rangle)$ , we can recast the above sensitivities to the New Physics operator scale  $\Lambda_{\text{NP}}$ :  $\Lambda_{\text{NP}} \approx 400 \text{ TeV}$  (CMS reinterpretation),  $\Lambda_{\text{NP}} \approx 600 \text{ TeV}$  (HL-LHC with CMS trigger) and  $\Lambda_{\text{NP}} \approx 4000 \text{ TeV}$  (HL-LHC with soft trigger), applicable for a RHN with  $m_N = 40 \text{ GeV}$  and  $|V_{\ell N}|^2 = 10^{-12}$ . These are already comparable to prospects at future lepton colliders [92].

As discussed in Sec. II B, the exotic Higgs production channel  $pp \rightarrow \Phi \rightarrow NN$  can have a large cross section and is nearly unsuppressed by the Higgs mixing  $\sin \alpha$  for  $m_h < m_\Phi \lesssim 150 \text{ GeV}$ . Consequently, the current constraint and the future sensitivity are even better than for SM Higgs production, as shown in Fig. 2 (right). The same parameters and scenarios are considered as above, with an exotic Higgs mass of  $m_\Phi = 150 \text{ GeV}$ . As can be seen, a reduction of the Higgs mixing from  $\sin \alpha = 0.24$  to 0.14 has little impact due to the decreased sensitivity on the mixing. Hence, the weakest Higgs mixing that still results in a 95% CL signal can be as small as  $\sin \alpha = 0.07$  (CMS reinterpretation), 0.02 (HL-LHC with CMS trigger) and 0.002 (HL-LHC with soft trigger).

## V. CONCLUSION

The origin of neutrino masses remains an open issue in particle physics. Although the seesaw mechanism provides an elegant solution, the right-handed neutrinos (RHNs) it predicts are difficult to probe at colliders. This is because the active-sterile mixing is required to be small to generate

light neutrino masses in the canonical seesaw. We instead consider that Majorana RHN masses are generated by the spontaneous symmetry breaking of a  $B - L$  gauge symmetry, under which the RHNs are charged. The RHNs can then be produced abundantly at colliders but remain long-lived due to the small active-sterile mixing strengths.

A search for the LLPs has been performed at CMS, using the displaced shower signature in its muon system [60]. We have reinterpreted it as a search for RHNs in the  $B - L$  gauge model, produced via  $pp \rightarrow Z', Z, h, \Phi \rightarrow NN$  and decaying at displaced vertices in the CMS endcap. We found that by applying the same trigger and reconstruction, the Higgs portals  $h$  and  $\Phi$  can be used to probe RHNs with masses  $m_N \approx 40$  GeV and active-sterile mixing strengths  $|V_{\ell N}|^2 \approx 10^{-12}$  using existing CMS data and for  $B - L$  model parameters satisfying current constraints. The gauge portals  $Z$  and  $Z'$  offer less promise in the near future.

Our results illustrate that searches for displaced showers in the CMS muon system are powerful probes to reveal the origin of neutrino masses. Existing CMS data is already excluding yet unexplored parameter space in the well-motivated  $B - L$  gauge model that covers the canonical seesaw floor, i.e., where a light neutrino mass scale of the order  $10^{-2}$  eV  $\lesssim m_\nu \lesssim 0.5$  eV is generated. The work motivates a dedicated search for displaced showers in the muon system with potential optimizations applied, such as for 3-body decay modes relevant for our RHN signatures.

### Acknowledgments

W. L. is supported by National Natural Science Foundation of China (Grant No.12205153). S. K. is supported by the FWF research group grant FG1 and FWF project number P 36947-N. F.F.D. acknowledges support from the UK Science and Technology Facilities Council (STFC) via the Consolidated Grants ST/P00072X/1 and ST/T000880/1.

### Appendix A: The Minimal $B - L$ Gauge Model

We here briefly summarize the minimal  $B - L$  gauge model, and the constraints on relevant model parameters. The  $B - L$  model extends the SM gauge group with the additional  $B - L$  symmetry,  $SU(3)_c \times SU(2)_L \times U(1)_Y \times U(1)_{B-L}$ . The particle content is also extended, by including the  $B - L$  gauge boson  $Z'$ , three fermionic Weyl RHNs  $\nu_R^i$  and the  $B - L$  Higgs  $\Phi$ . The relevant Lagrangian

in the interaction eigenstates is

$$\begin{aligned}
\mathcal{L}_{B-L} = & -\frac{1}{4}Z'_{\mu\nu}Z'^{\mu\nu} + D_\mu\Phi^*D^\mu\Phi + \sum_i \bar{\nu}_R^i i \not{D}\nu_R^i \\
& - \frac{\epsilon}{2}B^{\mu\nu}Z'_{\mu\nu} \{+m_{Z'}^2 B^\mu Z'_\mu\} \\
& - \frac{1}{2}\sum_{i,j} \left( \lambda_N^{ij} \bar{\nu}_R^{i,c} \Phi \nu_R^j + \text{h.c.} \right) \\
& - \sum_{\alpha,j} \left( \lambda_D^{\alpha j} \bar{L}^\alpha \cdot \tilde{H} \nu_R^j + \text{h.c.} \right) - \mathcal{V}(H, \Phi), \tag{A.1}
\end{aligned}$$

with the field strength tensor of the  $B - L$  gauge group  $Z'_{\mu\nu} = \partial_\mu Z'_\nu - \partial_\nu Z'_\mu$ , the hypercharge,  $B_{\mu\nu} = \partial_\mu B_\nu - \partial_\nu B_\mu$ , and the covariant derivative  $D_\mu = D_\mu^{\text{SM}} - ig_{B-L}Q_{B-L}Z'_\mu$ , including the  $B - L$  contribution, with  $g_{B-L}$  and  $Q_{B-L}$  being the  $B - L$  gauge coupling and charge, respectively. In Eq. (A.1),  $H$  is the SM Higgs doublet, with  $\tilde{H} = i\sigma^2 H^*$  and  $L^\alpha$  are the SM lepton doublets. The SM particles have their canonical  $Q_{B-L}$  charges while that of the exotic particles take the values  $Q_{B-L}(Z') = 0$ ,  $Q_{B-L}(\nu_{Ri}) = -1$  and  $Q_{B-L}(\Phi) = 2$ , while they are singlets under the SM gauge symmetries.

### 1. Higgs Sector

In Eq. (A.1),  $\mathcal{V}(H, \Phi)$  is the scalar potential

$$\begin{aligned}
\mathcal{V}(H, \Phi) = & m^2 H^\dagger H + \mu^2 |\Phi|^2 + \lambda_1 (H^\dagger H)^2 \\
& + \lambda_2 |\Phi|^4 + \lambda_3 H^\dagger H |\Phi|^2. \tag{A.2}
\end{aligned}$$

Both the SM and  $B - L$  Higgs acquire vacuum expectation values,  $v = \langle H^0 \rangle$ ,  $v_{B-L} = \langle \Phi \rangle$ , leading to a breaking of the model's gauge group to  $SU(3)_c \times U(1)_{\text{EM}}$ . In addition, the scalar potential in Eq. (A.2) gives rise to the mass matrix of the Higgs fields ( $H^0, \Phi$ ) at tree level [93],

$$M_H^2 = \begin{pmatrix} 2\lambda_1 v^2 & \lambda_3 v_{B-L} v \\ \lambda_3 v_{B-L} v & 2\lambda_2 v_{B-L}^2 \end{pmatrix}. \tag{A.3}$$

The Higgs masses at tree level are

$$\begin{aligned}
M_{h,\Phi}^2 = & \lambda_1 v^2 + \lambda_2 v_{B-L}^2 \\
& - (+)\sqrt{(\lambda_1 v^2 - \lambda_2 v_{B-L}^2)^2 + (\lambda_3 v_{B-L} v)^2}, \tag{A.4}
\end{aligned}$$

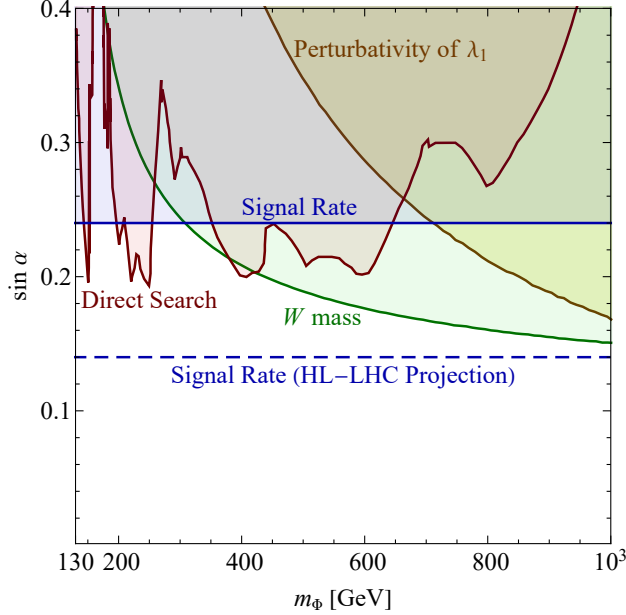


FIG. 3: Current limits on the Higgs mixing strength  $\sin \alpha$ , adapted from [94]. The bound from measuring the Higgs signal rate has been updated using the LHC Run 2 results [94–96]. Their projection at the HL-LHC with  $3000 \text{ fb}^{-1}$  integrated luminosity, taking the uncertainty  $\delta\mu = |1 - \sigma(pp \rightarrow h)/\sigma(pp \rightarrow h)_{\text{SM}}| = 0.02$ , is shown for comparison [90, 91].

with the mixing given by

$$\begin{pmatrix} h \\ \Phi' \end{pmatrix} = \begin{pmatrix} \cos \alpha & -\sin \alpha \\ \sin \alpha & \cos \alpha \end{pmatrix} \begin{pmatrix} H^0 \\ \Phi \end{pmatrix}, \quad (\text{A.5})$$

where the mixing angle  $\alpha$  is given through

$$\tan(2\alpha) = \frac{\lambda_3 v_{B-L} v}{\lambda_2 v_{B-L}^2 - \lambda_1 v^2}. \quad (\text{A.6})$$

We take  $m_h = m_{H^0} \approx 125 \text{ GeV} < m_\Phi$  where we drop the prime on the mass eigenstate<sup>1</sup>.

A summary of recent experimental limits on the Higgs mixing within an exotic singlet scalar can be found in [94]. The Higgs mixing can be probed by direct searches for a heavy scalar and a measurement of the Higgs signal rate [93, 94, 97]. The existence of an additional scalar also introduces a shift to the  $W$  boson mass [95, 98]. A limit from the  $W$  boson mass is derived

<sup>1</sup> The case where  $m_\Phi < m_h$  is considered in [55].

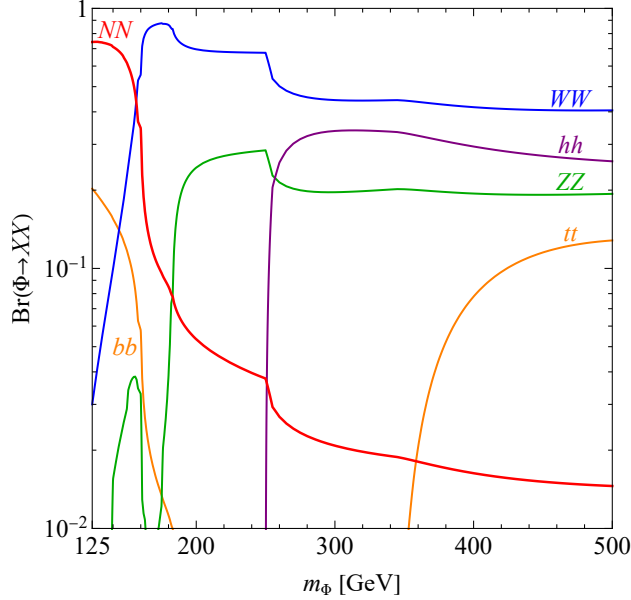


FIG. 4: Decay branching ratios of the  $B-L$  Higgs  $\Phi$  as a function of its mass  $m_\Phi$ . A single RHN with mass  $m_N = 0.3 \times m_\Phi$  is assumed and the Higgs mixing strength is taken as  $\sin \alpha = 0.08$ . The  $B-L$  Higgs VEV is fixed at  $\langle \Phi \rangle = 3.75$  TeV.

by comparing the experimental Particle Data Group value,  $m_W^{\text{exp}} = 80.379 \pm 0.012$  GeV and the SM predicted value,  $m_W^{\text{SM}} = 80.356$  GeV [99]. Lastly, requiring the scalar coupling  $\lambda_1$  to remain perturbative can also be used to infer a limit on the mixing. From Ref. [94, 95] using LHC Run 2 results [96], an upper limit from the signal rate can be obtained at  $\sin \alpha \lesssim 0.24$ . At the 14 TeV HL-LHC with  $3000 \text{ fb}^{-1}$  integrated luminosity, a measurement of the Higgs signal rate is expected to achieve an uncertainty of  $\delta\mu = |1 - \sigma(pp \rightarrow h)/\sigma(pp \rightarrow h)_{\text{SM}}| = 0.02$  [90, 91], with a projected sensitivity on the Higgs mixing of  $\sin \alpha \approx 0.14$ .

Besides SM Higgs production at the LHC, we also consider the production of the  $B-L$  Higgs  $\Phi$  with subsequent decay to RHNs. The branching ratios of  $\Phi$  to relevant decay products is shown in Fig. 4 as a function of its mass, calculated in MadGraph for the  $B-L$  gauge model. The  $B-L$  Higgs decays to SM final states as well as a pair of RHNs  $\Phi \rightarrow NN$  where we take the RHN mass  $m_N = 0.3 \times m_\Phi$  that approximately maximizes the partial decay rate. The decays to SM particles are suppressed by the Higgs mixing which is taken at a small value  $\sin \alpha = 0.08$  in the figure to illustrate the potential dominance of the decay  $\Phi \rightarrow NN$  for  $m_\Phi \lesssim 160$  GeV. The  $B-L$  Higgs VEV is fixed at  $\langle \Phi \rangle = 3.75$  TeV. As noted in the main section, as long as  $\Phi \rightarrow NN$  is not

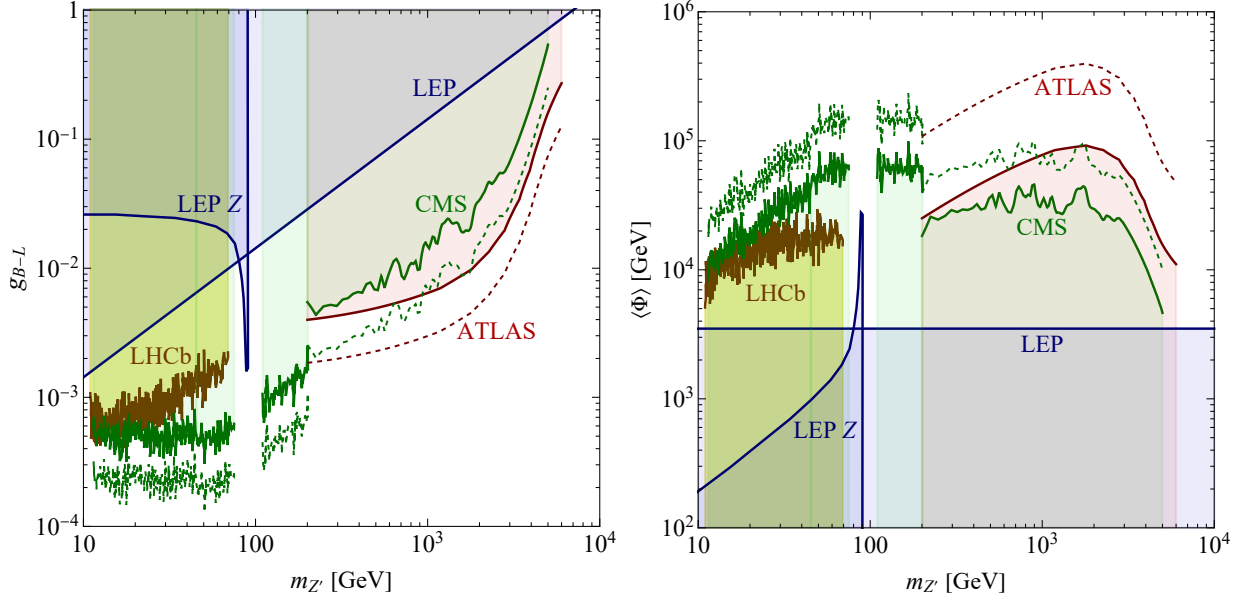


FIG. 5: Current limits on the  $B - L$  gauge coupling  $g_{B-L}$  (left) and the  $B - L$  VEV  $\langle\Phi\rangle = m_{Z'}/(2g_{B-L})$  (right) as a function of the  $Z'$  mass  $m_{Z'}$  from resonance searches at CMS [41, 44, 100–102], ATLAS [41, 66], LHCb [103], electroweak precision tests [73, 104] and searches for invisible  $Z'$  final states [105] (LEP). Also shown are the projected sensitivities at ATLAS and CMS for the  $3000 \text{ fb}^{-1}$  HL-LHC.

dominant, the cross section  $\sigma(pp \rightarrow \Phi \rightarrow NN)$  is largely independent of the Higgs mixing as it cancels out between production and decay. As can be seen,  $\text{Br}(\Phi \rightarrow NN) \approx 0.5 - 0.85$  is large for  $m_\Phi \lesssim 2m_W \approx 160 \text{ GeV}$ .

## 2. Gauge Sector

Arguably the most direct way to probe the  $B - L$  model is through extra gauge boson with mass  $m_{Z'} = 2g_{B-L}v_{B-L}$ . In Fig. 5 (left), the current limits and projected sensitivities on the gauge coupling  $g_{B-L}$  as a function of  $m_{Z'}$  are shown. For the parameter space of our interests,  $10 \text{ GeV} < m_{Z'} < 10 \text{ TeV}$ , the existing limits mainly arise from colliders through searches at CMS, ATLAS and LHCb, as well as EW precision tests and searches of invisible final states of  $Z'$ . Limits from the LHCb were originally presented for a dark photon but can be reinterpreted in the  $B - L$  model, following [106]. The limits from EW precision tests (LEP) are effectively on the vacuum expectation value of the  $B - L$  Higgs with  $v_{B-L} = m_{Z'}/(2g_{B-L}) \gtrsim 3.5 \text{ TeV}$  [73, 104]. For light



$Z'$  with  $10 \text{ GeV} < m_{Z'} < m_W$ , limits are from resonance searches for di-leptons final states at LHCb [103] and CMS [100, 101]. The current limits are  $g_{B-L} \lesssim 6 \times 10^{-4}$ . When  $m_{Z'} \sim m_{W,Z}$ , there are large backgrounds from the SM gauge bosons, hence the limit from LEP become dominant, except for  $m_{Z'} \lesssim m_Z$  when the search of the invisible decay of  $Z'$  at LEP [105] is more stringent. The CMS search [100, 101] is effective for  $110 \text{ GeV} < m_{Z'} < 200 \text{ GeV}$ , with an upper limit of  $g_{B-L} \lesssim 10^{-3}$ . For heavier  $Z'$ , the limits from high mass resonance searches at CMS [102] and ATLAS [66], as well as LEP apply. Among them, the limits from ATLAS are the most stringent for  $m_{Z'} \lesssim 6 \text{ TeV}$ . Due to the large mass, the background from the SM gauge bosons is suppressed and the limits become less stringent as  $Z'$  becomes heavier, reaching  $g_{B-L} \lesssim 0.2$  when  $m_{Z'} \approx 6 \text{ TeV}$ . For even heavier  $Z'$ , one can only rely on the limits from LEP. We also show the estimated sensitivities of ATLAS and CMS at the HL-LHC with  $3000 \text{ fb}^{-1}$ , by scaling the current bounds with luminosity as  $g_{B-L} \propto \text{luminosity}^{-1/4}$ . The same constraints are displayed in Fig. 5 (right), but interpreted with respect to the  $B-L$  VEV  $v_{B-L} = \langle \Phi \rangle = m_{Z'}/(2g_{B-L})$ .

In the minimal  $B-L$  model, no kinetic or mass mixing between the SM hypercharge and  $B-L$  is considered. Kinetic mixing is incorporated by including the  $\epsilon$  term in Eq. (A.1) [68]. The mass mixing term  $m_{ZZ'}^2$  violates the model's gauge symmetry but may still be present if the  $B-L$  and electroweak symmetry breaking are connected in a broader framework. For our purposes, we take  $\epsilon$  and  $m_{ZZ'}^2$  as effective, independent parameters at the electroweak scale. The mass mixing induces a field mixing angle  $\gamma$  between the two gauge bosons,

$$\tan \gamma = \frac{m_{ZZ'}^2}{m_{Z'}^2 - m_Z^2}, \quad (\text{A.7})$$

and both kinetic and mass mixing lead to a coupling of the SM-like gauge boson to the  $B-L$  current  $J_{B-L}^\mu$  [107],  $-\sin \theta_{ZZ'} Z_\mu J_{B-L}^\mu$ , with the overall mixing angle

$$\sin \theta_{ZZ'} \approx \tan \gamma + \frac{\epsilon \sin \theta_W}{m_{Z'}^2/m_Z^2 - 1}, \quad (\text{A.8})$$

for  $\epsilon$  and  $\gamma$  sufficiently small. Here,  $\theta_W$  is the electroweak mixing angle. Gauge boson mixing induces an additional parity-violating asymmetry and is thus constrained by precise measurements of atomic parity violation, with  $\beta = g_{B-L} \sin \theta_{ZZ'} \lesssim 10^{-3}$  [68]. This leads to a potential change in the  $Z$  production cross section by a factor of  $\beta^2 \sim 10^{-6}$ , still allowed at the LHC since the uncertainty of the  $Z$  production cross section is about 4% [108, 109].

### 3. Neutrino Sector

The Yukawa matrix  $y_N$  in Eq. (A.1) gives rise to the RHN masses, generated in breaking the  $B - L$  symmetry, with the mass matrix given by  $m_N = y_N \langle \Phi \rangle$ . Likewise, the active neutrinos mix with the RHNs via the Dirac mass matrix  $m_D = y_\nu v / \sqrt{2}$ . The complete mass matrix in the  $(\nu_L^c, \nu_R)$  basis is then

$$\mathcal{M} = \begin{pmatrix} 0 & m_D \\ m_D^T & M_N \end{pmatrix}, \quad (\text{A.9})$$

Here,  $v = \langle H^0 \rangle \approx 246$  GeV and  $v_{B-L} = \langle \Phi \rangle$  are the vacuum expectation values for electroweak and  $B - L$  symmetry breaking, respectively. In the seesaw limit,  $M_N \gg m_D$ , the light neutrino masses are

$$m_\nu \sim -m_D M_N^{-1} m_D^T. \quad (\text{A.10})$$

The flavour and mass eigenstates of the light and heavy neutrinos are related as

$$\begin{pmatrix} \nu_L^c \\ \nu_R \end{pmatrix} = \begin{pmatrix} U & V_{\ell N} \\ V_{N\ell} & U_N \end{pmatrix} \begin{pmatrix} \nu^c \\ N \end{pmatrix}. \quad (\text{A.11})$$

The mixing and the light neutrino masses are constrained by oscillation experiments, namely, the charged current lepton mixing  $U \approx U_{\text{PMNS}}$ , apart from small non-unitarity corrections. For simplicity, we assume the presence of a single RHN  $N$  mixing with a single lepton flavour at a time. This relates the light neutrino mass scale  $m_\nu$  with the RHN mass  $m_N$  as  $m_\nu = |V_{\ell N}|^2 m_N$ . While this simplification does not allow to describe the full light neutrino phenomenology, the mass should not exceed limits on the absolute neutrino mass scale currently set by the KATRIN experiment as  $m_\nu < 0.45$  eV at 90 % CL [87]. While not a strict lower limit, observations of the solar neutrino oscillation length indicate a smallest non-vanishing neutrino mass scale of  $\sqrt{\Delta m_{\text{sol}}^2} = 9 \times 10^{-3}$  eV [88]. We thus take the range  $9 \times 10^{-3}$  eV  $< |V_{\ell N}|^2 m_N < 0.45$  eV as a target to probe the canonical seesaw floor of neutrino mass generation.

RHNs can be searched for through their mixing  $V_{\ell N}$  with the active neutrinos, via their resulting participation in SM neutral and charged-current interactions, irrespective of the presence of a  $B - L$  gauge interaction. This leads to a wide range of constraints at colliders, in beam dump experiments, meson decay searches, etc.. In the figures in the main text, we display current constraints compiled

in [29] for comparison with our production mechanisms. The focus of future efforts is on the RHN lifetime frontier and we display the projected sensitivities of SHiP [110], CMS [111] and FCC-ee [112] as representative examples in our parameter space of interest.

- 
- [1] R. Davis, *Prog. Part. Nucl. Phys.* **32**, 13 (1994).
  - [2] Y. Fukuda et al. (Super-Kamiokande), *Phys. Rev. Lett.* **81**, 1562 (1998), hep-ex/9807003.
  - [3] K. Eguchi et al. (KamLAND), *Phys. Rev. Lett.* **90**, 021802 (2003), hep-ex/0212021.
  - [4] P. Minkowski, *Phys. Lett. B* **67**, 421 (1977).
  - [5] M. Fukugita and T. Yanagida, *Phys. Lett. B* **174**, 45 (1986).
  - [6] M. A. Luty, *Phys. Rev. D* **45**, 455 (1992).
  - [7] S. Davidson, E. Nardi, and Y. Nir, *Phys. Rept.* **466**, 105 (2008), 0802.2962.
  - [8] K. Bondarenko, A. Boyarsky, D. Gorbunov, and O. Ruchayskiy, *JHEP* **11**, 032 (2018), 1805.08567.
  - [9] D. A. Bryman and R. Shrock, *Phys. Rev. D* **100**, 073011 (2019), 1909.11198.
  - [10] S. Balaji, M. Ramirez-Quezada, and Y.-L. Zhou, *JHEP* **04**, 178 (2020), 1910.08558.
  - [11] W. Liu, K.-P. Xie, and Z. Yi, *Phys. Rev. D* **105**, 095034 (2022), 2109.15087.
  - [12] A. M. Abdullahi et al., *J. Phys. G* **50**, 020501 (2023), 2203.08039.
  - [13] Y. Zhang and W. Liu, *Phys. Rev. D* **107**, 095031 (2023), 2301.06050.
  - [14] D. Barducci, W. Liu, A. Titov, Z. S. Wang, and Y. Zhang, *Phys. Rev. D* **108**, 115009 (2023), 2308.16608.
  - [15] W. Liu and F. F. Deppisch (2023), 2312.11165.
  - [16] S. Chatrchyan et al. (CMS), *Phys. Lett. B* **717**, 109 (2012), 1207.6079.
  - [17] R. Aaij et al. (LHCb), *Phys. Rev. Lett.* **112**, 131802 (2014), 1401.5361.
  - [18] G. Aad et al. (ATLAS), *JHEP* **07**, 162 (2015), 1506.06020.
  - [19] V. Khachatryan et al. (CMS), *Phys. Lett. B* **748**, 144 (2015), 1501.05566.
  - [20] V. Khachatryan et al. (CMS), *JHEP* **04**, 169 (2016), 1603.02248.
  - [21] E. Cortina Gil et al. (NA62), *Phys. Lett. B* **778**, 137 (2018), 1712.00297.
  - [22] A. M. Sirunyan et al. (CMS), *Phys. Rev. Lett.* **120**, 221801 (2018), 1802.02965.
  - [23] A. M. Sirunyan et al. (CMS), *JHEP* **01**, 122 (2019), 1806.10905.
  - [24] G. Aad et al. (ATLAS), *JHEP* **10**, 265 (2019), 1905.09787.
  - [25] R. Aaij et al. (LHCb), *Eur. Phys. J. C* **81**, 248 (2021), 2011.05263.
  - [26] A. Tumasyan et al. (CMS), *JHEP* **07**, 081 (2022), 2201.05578.
  - [27] G. Aad et al. (ATLAS), *Eur. Phys. J. C* **83**, 824 (2023), 2305.14931.
  - [28] A. Hayrapetyan et al. (CMS), *Phys. Rev. D* **110**, 012004 (2024), 2402.18658.

- [29] P. D. Bolton, F. F. Deppisch, and P. S. Bhupal Dev, *JHEP* **03**, 170 (2020), 1912.03058.
- [30] A. Davidson, *Phys. Rev. D* **20**, 776 (1979).
- [31] R. N. Mohapatra and R. E. Marshak, *Phys. Rev. Lett.* **44**, 1316 (1980), [Erratum: *Phys.Rev.Lett.* **44**, 1643 (1980)].
- [32] S. Iso, N. Okada, and Y. Orikasa, *Phys. Lett. B* **676**, 81 (2009), 0902.4050.
- [33] S. Iso, N. Okada, and Y. Orikasa, *Phys. Rev. D* **80**, 115007 (2009), 0909.0128.
- [34] I. Baldes and M. O. Olea-Romacho, *JHEP* **01**, 133 (2024), 2307.11639.
- [35] F. F. Deppisch, N. Desai, and J. W. F. Valle, *Phys. Rev. D* **89**, 051302 (2014), 1308.6789.
- [36] B. Batell, M. Pospelov, and B. Shuve, *JHEP* **08**, 052 (2016), 1604.06099.
- [37] F. Deppisch, S. Kulkarni, and W. Liu, *Phys. Rev. D* **100**, 035005 (2019), 1905.11889.
- [38] E. Accomando, L. Delle Rose, S. Moretti, E. Olaiya, and C. H. Shepherd-Themistocleous, *JHEP* **02**, 109 (2018), 1708.03650.
- [39] A. Das, P. S. B. Dev, and N. Okada, *Phys. Lett. B* **799**, 135052 (2019), 1906.04132.
- [40] K. Cheung, K. Wang, and Z. S. Wang, *JHEP* **09**, 026 (2021), 2107.03203.
- [41] C.-W. Chiang, G. Cottin, A. Das, and S. Mandal, *JHEP* **12**, 070 (2019), 1908.09838.
- [42] P. Fileviez Pérez and A. D. Plascencia, *Phys. Rev. D* **102**, 015010 (2020), 2005.04235.
- [43] A. Das, N. Okada, S. Okada, and D. Raut, *Phys. Lett. B* **797**, 134849 (2019), 1812.11931.
- [44] W. Liu, S. Kulkarni, and F. F. Deppisch, *Phys. Rev. D* **105**, 095043 (2022), 2202.07310.
- [45] C. Han, T. Li, and C.-Y. Yao, *Phys. Rev. D* **104**, 015036 (2021), 2103.03548.
- [46] A. Das and N. Okada, *Phys. Lett. B* **774**, 32 (2017), 1702.04668.
- [47] M. L. Graesser, *Phys. Rev. D* **76**, 075006 (2007), 0704.0438.
- [48] A. Maiezza, M. Nemevšek, and F. Nesti, *Phys. Rev. Lett.* **115**, 081802 (2015), 1503.06834.
- [49] F. F. Deppisch, W. Liu, and M. Mitra, *JHEP* **08**, 181 (2018), 1804.04075.
- [50] J. D. Mason, *JHEP* **07**, 089 (2019), 1905.07772.
- [51] E. Accomando, L. Delle Rose, S. Moretti, E. Olaiya, and C. H. Shepherd-Themistocleous, *JHEP* **04**, 081 (2017), 1612.05977.
- [52] Y. Gao, M. Jin, and K. Wang, *JHEP* **02**, 101 (2020), 1904.12325.
- [53] A. M. Gago, P. Hernández, J. Jones-Pérez, M. Losada, and A. Moreno Briceño, *Eur. Phys. J. C* **75**, 470 (2015), 1505.05880.
- [54] J. Jones-Pérez, J. Masias, and J. D. Ruiz-Álvarez, *Eur. Phys. J. C* **80**, 642 (2020), 1912.08206.
- [55] W. Liu, J. Li, J. Li, and H. Sun, *Phys. Rev. D* **106**, 015019 (2022), 2204.03819.
- [56] J. Li, W. Liu, and H. Sun, *Phys. Rev. D* **109**, 035022 (2024), 2309.05020.
- [57] F. F. Deppisch, S. Kulkarni, and W. Liu (2023), 2311.01719.
- [58] N. Bernal, K. Deka, and M. Losada (2023), 2311.18033.

- [59] A. Atre, T. Han, S. Pascoli, and B. Zhang, JHEP **05**, 030 (2009), 0901.3589.
- [60] A. Tumasyan et al. (CMS), Phys. Rev. Lett. **127**, 261804 (2021), 2107.04838.
- [61] M. Aaboud et al. (ATLAS), Phys. Rev. D **99**, 052005 (2019), 1811.07370.
- [62] G. Aad et al. (ATLAS), Phys. Rev. D **101**, 052013 (2020), 1911.12575.
- [63] G. Aad et al. (ATLAS), JHEP **2306**, 200 (2023), 2301.13866.
- [64] Z. S. Wang (2024), 2406.16281.
- [65] G. Cottin, J. C. Helo, M. Hirsch, C. Peña, C. Wang, and S. Xie, JHEP **02**, 011 (2023), 2210.17446.
- [66] G. Aad et al. (ATLAS), Phys. Lett. B **796**, 68 (2019), 1903.06248.
- [67] M. Aaboud et al. (ATLAS), JHEP **02**, 117 (2017), 1612.03636.
- [68] P. S. B. Dev, W. Rodejohann, X.-J. Xu, and Y. Zhang, JHEP **06**, 039 (2021), 2103.09067.
- [69] CERN, *Cern yellow reports 13 tev*, <https://twiki.cern.ch/twiki/bin/view/LHCPhysics/CERNYellowReportPageAt13TeV>.
- [70] *Lhc higgs cross section working group*, <https://twiki.cern.ch/twiki/bin/view/LHCPhysics/HiggsEuropeanStrategy>.
- [71] D. de Florian et al. (LHC Higgs Cross Section Working Group), **2/2017** (2016), 1610.07922.
- [72] M. Cacciari, G. P. Salam, and G. Soyez, Eur. Phys. J. C **72**, 1896 (2012), 1111.6097.
- [73] J. Alcaraz et al. (ALEPH, DELPHI, L3, OPAL, LEP Electroweak Working Group) (2006), hep-ex/0612034.
- [74] C. Degrande, C. Duhr, B. Fuks, D. Grellscheid, O. Mattelaer, and T. Reiter, Comput. Phys. Commun. **183**, 1201 (2012), 1108.2040.
- [75] J. Alwall, R. Frederix, S. Frixione, V. Hirschi, F. Maltoni, O. Mattelaer, H. S. Shao, T. Stelzer, P. Torrielli, and M. Zaro, JHEP **07**, 079 (2014), 1405.0301.
- [76] M. L. Mangano, M. Moretti, F. Piccinini, and M. Treccani, JHEP **01**, 013 (2007), hep-ph/0611129.
- [77] S. Hoeche, F. Krauss, N. Lavesson, L. Lonnblad, M. Mangano, A. Schaliche, and S. Schumann, in *HERA and the LHC: A Workshop on the Implications of HERA for LHC Physics: CERN - DESY Workshop 2004/2005 (Midterm Meeting, CERN, 11-13 October 2004; Final Meeting, DESY, 17-21 January 2005)* (2005), pp. 288–289, hep-ph/0602031.
- [78] T. Sjöstrand, S. Ask, J. R. Christiansen, R. Corke, N. Desai, P. Ilten, S. Mrenna, S. Prestel, C. O. Rasmussen, and P. Z. Skands, Comput. Phys. Commun. **191**, 159 (2015), 1410.3012.
- [79] J. de Favereau, C. Delaere, P. Demin, A. Giammanco, V. Lemaître, A. Mertens, and M. Selvaggi (DELPHES 3), JHEP **02**, 057 (2014), 1307.6346.
- [80] A. Hayrapetyan et al. (CMS) (2024), 2402.01898.
- [81] C. Wang, *Dedicated Delphes Module*, <https://github.com/delphes/delphes/pull/103> (2022).
- [82] CMS Collaboration, *Search for long-lived particles decaying in the CMS endcap muon detectors in*

- proton-proton collisions at  $\sqrt{s} = 13$  TeV (Version 2)*, [HEPData \(collection\)](#) (2021).
- [83] J. Alwall, M. Herquet, F. Maltoni, O. Mattelaer, and T. Stelzer, *JHEP* **06**, 128 (2011), 1106.0522.
- [84] S. P. Jones, M. Kerner, and G. Luisoni, *Phys. Rev. Lett.* **120**, 162001 (2018), [Erratum: *Phys.Rev.Lett.* **128**, 059901 (2022)], 1802.00349.
- [85] K. Becker et al., *SciPost Phys. Core* **7**, 001 (2024), 2005.07762.
- [86] F. Maltoni, E. Vryonidou, and M. Zaro, *JHEP* **11**, 079 (2014), 1408.6542.
- [87] M. Aker et al. (Katrin) (2024), 2406.13516.
- [88] I. Esteban, M. C. Gonzalez-Garcia, M. Maltoni, T. Schwetz, and A. Zhou, *JHEP* **09**, 178 (2020), 2007.14792.
- [89] P. D. Bolton, F. F. Deppisch, and P. S. B. Dev, in *56th Rencontres de Moriond on Electroweak Interactions and Unified Theories* (2022), 2206.01140.
- [90] M. Cepeda et al., *CERN Yellow Rep. Monogr.* **7**, 221 (2019), 1902.00134.
- [91] ATLAS and CMS, *CERN Yellow Rep. Monogr.* **7**, Addendum (2019), 1902.10229.
- [92] D. Barducci, E. Bertuzzo, A. Caputo, P. Hernandez, and B. Mele, *JHEP* **03**, 117 (2021), 2011.04725.
- [93] T. Robens and T. Stefaniak, *Eur. Phys. J. C* **75**, 104 (2015), 1501.02234.
- [94] T. Robens, *Springer Proc. Phys.* **292**, 141 (2023), 2209.15544.
- [95] A. Papaefstathiou, T. Robens, and G. White, in *Snowmass 2021* (2022), 2205.14379.
- [96] ATLAS, *Combined measurements of Higgs boson production and decay using up to 139 fb<sup>-1</sup> of proton-proton collision data at  $\sqrt{s} = 13$  TeV collected with the ATLAS experiment* (2021).
- [97] T. Robens, in *55th Rencontres de Moriond on QCD and High Energy Interactions* (2021), 2105.07719.
- [98] D. López-Val and T. Robens, *Phys. Rev. D* **90**, 114018 (2014), 1406.1043.
- [99] R. L. Workman et al. (Particle Data Group), *PTEP* **2022**, 083C01 (2022).
- [100] CMS, *Search for a narrow resonance decaying to a pair of muons in proton-proton collisions at 13 TeV* (2019).
- [101] A. M. Sirunyan et al. (CMS), *Phys. Rev. Lett.* **124**, 131802 (2020), 1912.04776.
- [102] A. M. Sirunyan et al. (CMS), *JHEP* **07**, 208 (2021), 2103.02708.
- [103] R. Aaij et al. (LHCb), *Phys. Rev. Lett.* **124**, 041801 (2020), 1910.06926.
- [104] G. Cacciapaglia, C. Csaki, G. Marandella, and A. Strumia, *Phys. Rev. D* **74**, 033011 (2006), hep-ph/0604111.
- [105] P. J. Fox, R. Harnik, J. Kopp, and Y. Tsai, *Phys. Rev. D* **84**, 014028 (2011), 1103.0240.
- [106] P. Ilten, Y. Soreq, M. Williams, and W. Xue, *JHEP* **06**, 004 (2018), 1801.04847.
- [107] M. Lindner, F. S. Queiroz, W. Rodejohann, and X.-J. Xu, *JHEP* **05**, 098 (2018), 1803.00060.
- [108] G. Aad et al. (ATLAS), *Phys. Lett. B* **759**, 601 (2016), 1603.09222.
- [109] ATLAS, *Measurement of  $t\bar{t}$  and Z-boson cross sections and their ratio using pp collisions at  $\sqrt{s} = 13.6$*

*TeV with the ATLAS detector (2023).*

- [110] C. Ahdida et al. (SHiP), *JHEP* **04**, 077 (2019), 1811.00930.
- [111] M. Drewes and J. Hajer, *JHEP* **02**, 070 (2020), 1903.06100.
- [112] A. Blondel et al., *Front. in Phys.* **10**, 967881 (2022), 2203.05502.